J. Phase Equilib. Diffus. (2020) 41:654–671
https://doi.org/10.1007/s11669-020-00832-2

# Thermodynamic Database Development for the $ZrO_2$-MgO-$MnO_x$ System

**Ivan Saenko**[1] · **Olga Fabrichnaya**[1]

Submitted: 29 April 2020 / in revised form: 24 June 2020 / Published online: 2 September 2020


**Abstract** Thermodynamic description of the $ZrO_2$-MgO-$MnO_x$ was derived for the first time using available experimental data on phase relations in air and protective gas atmosphere. Solid solution phases were modelled using compound energy formalism. The liquid phase was described by the modified two-sublattice model for ionic liquid. Solubility of $ZrO_2$ was modelled in cubic spinel and MgO-MnO solid solution (halite structure) and therefore the Gibbs energies of Zr-containing endmembers were introduced. Ternary interaction parameters were introduced for halite, cubic spinel and cubic $ZrO_2$ to reproduce the stabilization of cubic $ZrO_2$ at temperatures below its stability in bounding systems and stabilization of cubic spinel at temperatures above its stability limit in the bounding systems. The obtained thermodynamic database was used to interpret results of differential thermal analysis.

**Keywords** magnesium oxide · manganese oxides · phase diagrams · thermodynamic modelling · zirconia

## 1 Introduction

Phase equilibria in the $ZrO_2$-MgO-$MnO_x$ system are of interest due to several possible applications. One of them is development of TRIP steel metal matrix composite material strengthened by particles of MgO partially stabilized zirconia (Mg-PSZ).[1] Manganese provides good adhesion bonding between the steel matrix and the Mg-PSZ ceramics.[2,3] On the other hand, manganese is one of the main alloying elements of the steel matrix and can substitute Mg in Mg-PSZ during processing of this metal matrix composite[2,4,5] thus influencing the stability of the Mg-PSZ structure. It was shown that due to Mg diffusion from Mg-PSZ into precipitate sites or the steel matrix the Mg-PSZ was destabilized and transformed into the monoclinic phase, while due to diffusion of Mn into $ZrO_2$ particles, grains at its boundary remained cubic or tetragonal.[5] Therefore, knowledge of phase relations in the $ZrO_2$-MgO-$MnO_x$ system is important to improve the stability of Mg-PSZ and its bonding to the steel matrix.

The other possible application of the $ZrO_2$-MgO-$MnO_x$ system is for directionally solidified eutectic materials since both bounding systems $ZrO_2$-MgO and $ZrO_2$-$MnO_x$ are known to form directionally solidified eutectics.[6,7]

The phase relations in the $ZrO_2$-MgO-$MnO_x$ system were experimentally studied by Pavlyuchkov et al.[8] for the first time. The investigations were carried out in air and inert gas atmosphere. It was shown that relatively small additions of $ZrO_2$ stabilize cubic spinel in the ternary system in air at temperatures exceeding its stability range in the MgO-$MnO_x$ bounding system and compositions substantially enriched by MgO. The addition of $ZrO_2$ also significantly extends the homogeneity range of halite (MgO-MnO solid solution) toward MnO solubility in air. It should be also noted that cubic $ZrO_2$-based solid solutions are stabilized in the $ZrO_2$-MgO-$MnO_x$ system down to lower temperatures in comparison with the bounding systems both in air and inert gas atmosphere.

The thermodynamic descriptions of the bounding systems are available in literature.[9–11] However the description of the $ZrO_2$-$MnO_x$ system needed to be

✉ Ivan Saenko
ivan.saenko@iww.tu-freiberg.de; ivan.s.s@bk.ru

1 Institute of Materials Science, Technical University Bergakademie Freiberg, Gustav-Zeuner-Str. 5, 09599 Freiberg, Germany

modified since the description of the Mn-O system accepted by Dilner et al.[11] was from work of Kjellqvist and Selleby[12] while the one accepted by Pavlyuchkov et al.[10] was from work of Grundy et al.[13] Though the phase diagram of the Mn-O system was very similar in both works, the description of Kjellqvist and Selleby[12] is more advanced as it takes into account species distribution in the $Mn_3O_4$ tetragonal and cubic spinel. Special attention should be given to the fact that the thermodynamic description of the bounding systems $ZrO_2$-$MnO_x$ and $ZrO_2$-MgO will be modified due to introducing $Zr^{+4}$ in spinel and halite models and this should cause only minimal change to the phase diagrams of the bounding systems. It should also be noted that stabilization of spinel and cubic $ZrO_2$ in the quaternary system outside its stability ranges in the bounding system would require introducing Zr containing end-members in spinel and halite as well as ternary interaction parameters in all above mentioned phases to reproduce experimental data. Though the thermodynamic descriptions of the bounding systems are available, the system $ZrO_2$-MgO-$MnO_x$ was not modelled so far.

The aim of the present work is to develop thermodynamic description of the $ZrO_2$-MgO-$MnO_x$ system which reproduces experimental data for the system. Some key DTA experiments are planned to verify the thermodynamic description.

## 2 Materials and Methods

Samples were prepared using the co-precipitation method followed by evaporation procedure. The zirconium acetate solution in acetic acid $Zr(CH_3COO)_4$ (99.99%, Sigma-Aldrich), aqueous solution of manganese nitrate $Mn(NO_3)_2$ (99.9%, Alfa Aesar) and magnesium nitrate hexahydrate $Mg(NO_3)_2 \cdot 6H_2O$ (99.97%, Alfa Aesar) have been used as the primary chemicals. A detailed description of the sample preparation route was presented in Ref. 8.

X-ray powder diffraction (XRD) was performed using the URD63 diffractometer (Seifert, FPM, Freiberg, Germany) equipped by graphite monochromator with CuKα radiation (α = 1.5418 Å). The goniometer of the diffractometer had Bragg–Brentano geometry. Rietveld refinement was applied using the Maud software[14] for the characterization of all measured diffraction patterns in order to obtain the volume fractions of present phases as well as lattice parameters. Microstructural investigations have been carried out using scanning electron microscopy combined with dispersive x-ray spectrometry (SEM/EDX; Leo1530, Carl Zeiss/Bruker AXS Mikroanalysis GmbH). Chemical compositions of samples, phases and eutectic compositions have been determined using an EDX detector with an accuracy of ± 4 mol.%. Differential thermal analysis coupled with thermogravimetry (DTA-TG) was performed using a Setsys Evolution 1750 device with

**Table 1** Phases in the Zr-Mn-Mg-O system

| Phase name and abbreviation | Space group | Thermodynamic model |
|---|---|---|
| $ZrO_2$ based solid solutions | | $(Zr^{+4}, Mg^{+2}, Mn^{+2}, Mn^{+3})_1(O^{-2}, Va)_2$ |
| cubic, c-$ZrO_2$ | Fm-3 m | |
| tetragonal, t-$ZrO_2$ | $P4_2/nmc$ | |
| monoclinic, m-$ZrO_2$ | $P2_1/c$ | |
| halite (H) | Fm-3 m | $(Mg^{+2}, Mn^{+2}, Mn^{+3}, Zr^{+4}, Va)_1(O^{-2})_1$ |
| α-spinel (αSp) | $I4_1/amd$ | $(Mg^{+2}, Mn^{+2}, Mn^{+3})_1(Mg^{+2}, Mn^{+2}, Mn^{+3}, Va)_2(Mg^{+2}, Mn^{+2}, Va)_2(O^{-2})_4$ |
| β-spinel (βSp) | * | $(Mg^{+2}, Mn^{+2})_1(Mg^{+2}, Mn^{+2}, Mn^{+3}, Zr^{+4}, Va)_2(Mg^{+2}, Mn^{+2}, Va)_2(O^{-2})_4$ |
| $Mn_2O_3$ | Ia-3 | $(Mn^{+3}, Mn^{+2})_2(O^{-2}, Va)_3(O^{-2}, Va)_1$ |
| $MnO_2$ | $P4_2/mnm$ | $(Mn^{+4})_1(O^{-2})_2$ |
| bcc | Im-3 m | $(Mg, Mn, Zr)_1(O, Va)_3$ |
| hcp | $P6_3/mnc$ | $(Mg, Mn, Zr)_1(O, Va)_{0.5}$ |
| fcc | Fm-3 m | $(Mg, Mn, Zr)_1(O, Va)_1$ |
| cbcc | I-43 m | $(Mg, Mn, Zr)_1(Va)_1$ |
| cub_A13 | $P4_132$ | $(Mg, Mn, Zr)_1(Va)_1$ |
| C14-$ZrMn_2$ (C14) | $P6_3/mmc$ | $(Zr, Mn)_2(Zr, Mn)_1$ |

* β-spinel is supposed to have a cubic structure. However, in the work of Pavlyuchkov et al.,[8] β-spinel has been identified by a tetragonal structure, which is very close to cubic symmetry

PtRh10% crucibles, a heating rate of 10 K $min^{-1}$ and He atmosphere.

## 3 Thermodynamic Modelling

As basis for the thermodynamic description of the $ZrO_2$-MgO-$MnO_x$ system, the modelling of the MgO-$MnO_x$ boundary system was accepted according to the work of Dilner et al.[11] The phase and their models are listed in Table 1. The liquid phase is described by modified two-sublattice model for ionic liquid,[15,16] while solid solutions are described by compound energy formalism.[17] $Zr^{+4}$ ions were introduced in the liquid phase, cubic spinel and halite phase. The thermodynamic descriptions of the $ZrO_2$-MgO[9] and MgO-$MnO_x$[11] systems are compatible. Only due to the introduction of $Zr^{+4}$ in the halite phase the boundary system should be checked to avoid noticeable solubility of $ZrO_2$ in halite. Due to using different species in the ionic liquid in the Mn-O system by Kjellqvist and Selleby[12] ($MnO_{1.5}$ neutral species in the anionic sublattice) and by Grundy et al.[13] ($Mn^{+3}$ in the cationic sublattice) which were subsequently accepted in the work of Dilner et al.[11] for the MgO-$MnO_x$ system and Pavlyuchkov et al.[10] for the $ZrO_2$-$MnO_x$ system, the liquid phase description appeared to be incompatible. Though there is no experimental evidence, which model is to be preferred the thermodynamic description of the liquid by Kjellqvist and Selleby[12] was accepted because of their advanced modelling of tetragonal and cubic spinel phases along with their good reproduction of the phase diagram and thermodynamic properties in the Mn-O system. Therefore, the description of the liquid phase should be modified in the $ZrO_2$-$MnO_x$ system. Due to the introduction of $Zr^{+4}$ in halite and βSp phases the solubility of $ZrO_2$ should be very small in the $ZrO_2$-$MnO_x$ system.

The thermodynamic model assuming two-sublattices was accepted for the three modifications of $ZrO_2$ solid solutions as in the bounding systems. The solubility of $Mg^{+2}$, $Mn^{+3}$ and $Mn^{+2}$ in the $ZrO_2$ solid solutions were first based on extrapolations from bounding systems and then ternary interaction parameters were introduced to the cubic $ZrO_2$ based solid solution (c-$ZrO_2$). The solubilities of $ZrO_2$ in cubic spinel (*β*Sp) and halite phases were experimentally established by Pavlyuchkov et al.[8] in the system $ZrO_2$-MgO-$MnO_x$. The thermodynamic description of t-$ZrO_2$ and m-$ZrO_2$ were combined based on descriptions of bounding systems because solubility of MgO and $MnO_x$ was rather small in these phases and no ternary parameters were necessary to reproduce phase relations involving these phases. Thermodynamic descriptions of c-$ZrO_2$, *β*Sp and halite were modified in comparison with extrapolations from the bounding systems. Ternary parameters and the Gibbs energy of end-members involving $Zr^{+4}$ were necessary to model the solubility of $ZrO_2$ in *β*Sp and halite and to reproduce phase relations involving c-$ZrO_2$, *β*Sp and halite. The description of liquid was based on extrapolations from bounding systems. This was enough to reproduce phase relations involving liquid. The description of other phases such as α-spinel, $Mn_2O_3$, $MnO_2$ and $Mg_6MnO_8$ were accepted from Ref 11 and were not modified further because phase equilibria studied in Ref 8 did not involve only these phases.

It should be noted that phase equilibria were investigated in the field of stability of cubic spinel phase, while it transformed to tetragonal spinel during cooling. For most compositions cubic spinel is not quenchable (except Mg-rich compositions). Tetragonal $ZrO_2$ in the studied system is not quenchable transforming to the monoclinic phase. To get the preserved $ZrO_2$ with cubic structure also fast cooling was required. Therefore, to interpret experimental results, it was assumed that phases such as cubic spinel, tetragonal and cubic $ZrO_2$ solid solutions transformed to their low-temperature modifications without composition change.

### 3.1 Liquid

Liquid phase was described using the modified two sublattice model for ionic liquid[15,16] with the formula $(Mg^{+2}, Mn^{+2}, Zr^{+4})_P(O^{-2}, Va^{-Q}, MnO_{1.5})_Q$, where P and Q are stoichiometric parameters changing with composition to keep electro-neutrality.

### 3.2 Cubic Spinel

Cubic spinel was described by the compound energy formalism assuming mixing in tetrahedral and octahedral sites also assuming that $Mg^{+2}$ and $Mn^{+2}$ can occupy part of octahedral sites which are normally vacant: $(Mg^{+2}, Mn^{+2})_1(Mg^{+2}, Mn^{+2}, Mn^{+3}, Mn^{+4}, Zr^{+4}, Va)_2(Mg^{+2}, Mn^{+2}, Va)_2(O^{-2})_4$. Therefore the model used in the work of Dilner et al.[11] was expanded by considering $Zr^{+4}$ cations occupying the octahedral sites. It was assumed that smaller tetrahedral sites cannot be occupied by large $Zr^{+4}$ cations. Therefore, six new end-members appeared. The Gibbs energy of two of them can be derived using the electro-neutrality reactions between end-member compounds:

$$\mathbf{Mg^{+2}Zr_2^{+4}Va_2O_4^{-2}} + Mg^{+2}Mg_2^{+2}Va_2O_4^{-2} = 2 \cdot Mg_2ZrO_4 \quad \text{(Eq 1)}$$

$$\mathbf{Mn^{+2}Zr_2^{+4}Va_2O_4^{-2}} + Mn^{+2}Mn_2^{+2}Va_2O_4^{-2} = 2 \cdot Mn_2ZrO_4 \quad \text{(Eq 2)}$$

$Mg_2ZrO_4$ and $Mn_2ZrO_4$ are inversed spinel, $Mg(Mg_{0.5}Zr_{0.5})_2O_4$ and $Mn(Mn_{0.5}Zr_{0.5})_2O_4$ are fictive compounds, both unstable in the boundary systems. The Gibbs energy for these fictive compounds were described as the sum of the Gibbs energy of the oxides $G_{ZrO2\_c} + 2 \cdot G_{MO} + Vn$, where M = $Mg^{+2}$ or $Mn^{+2}$ and Vn (n = 1, 2) stands values to be optimized in both bounding systems. The calculated phase diagrams should show very limited solubility of $ZrO_2$ in spinel in the case of the $ZrO_2$-$MnO_x$ system and avoid the spinel phase appearing in the $ZrO_2$-MgO system.

The Gibbs energy of inversed spinel in both systems can be written as following

$$G_{M_2ZrO_4} = 0.5 \cdot {}^{\circ}G_{M+2:Zr+4:Va:O-2} + 0.5 \cdot {}^{\circ}G_{M+2:M+2:Va:O-2} + 2 \cdot R \cdot T \cdot (0.5 \cdot \ln(0.5) + 0.5 \cdot \ln(0.5)) \quad \text{(Eq 3)}$$

Therefore, the Gibbs energy for the end-members $M^{+2}Zr_2^{+4}Va_2O_4^{-2}$ can be derived from Eq 1 and 2: ${}^{\circ}G_{M+2:Zr+4:Va:O-2} = 2 \cdot G_{M_2ZrO_4} - {}^{\circ}G_{M+2:M+2:Va:O-2} + 4 \cdot R \cdot T \cdot \ln(2)$, with the last term being the contribution from configurational entropy. The Gibbs energy of end-members $M^{+2}M_2^{+2}Va_2O_4^{-2}$ were accepted from Mn-Mg-O system.[11]

For other four end-members (in bold) the Gibbs energy can be obtained from reciprocal reactions involving end-members with known Gibbs energy:

$$Mg^{+2}Zr_2^{+4}Va_2O_4^{-2} + Mg^{+2}Mg_2^{+2}Mg_2^{+2}O_4^{-2} = Mg^{+2}Mg_2^{+2}Va_2O_4^{-2} + \mathbf{Mg^{+2}Zr_2^{+4}Mg_2^{+2}O_4^{-2}} \quad \text{(Eq 4)}$$

$$Mn^{+2}Zr_2^{+4}Va_2O_4^{-2} + Mn^{+2}Mn_2^{+2}Mn_2^{+2}O_4^{-2} = Mn^{+2}Mn_2^{+2}Va_2O_4^{-2} + \mathbf{Mn^{+2}Zr_2^{+4}Mn_2^{+2}O_4^{-2}} \quad \text{(Eq 5)}$$

$$Mg^{+2}Zr_2^{+4}Va_2O_4^{-2} + Mn^{+2}Zr_2^{+4}Mn_2^{+2}O_4^{-2} = Mn^{+2}Zr_2^{+4}Va_2O_4^{-2} + \mathbf{Mg^{+2}Zr_2^{+4}Mn_2^{+2}O_4^{-2}} \quad \text{(Eq 6)}$$

$$Mg^{+2}Zr_2^{+4}Mg_2O_4^{-2} + Mn^{+2}Zr_2^{+4}Mn_2^{+2}O_4^{-2} = Mg^{+2}Zr_2^{+4}Mn_2O_4^{-2} + \mathbf{Mn^{+2}Zr_2^{+4}Mg_2^{+2}O_4^{-2}} \quad \text{(Eq 7)}$$

The Gibbs energies of reciprocal reactions were assumed to be zero. However, in case of necessity they can be considered as deviating from zero and adjusted to reproduce experimental data.

### 3.3 Halite

Halite is a monoxide solid solution with NaCl structure. The thermodynamic description of the halite phase was accepted from Dilner et al.[11] assuming that the cations $Mg^{+2}$, $Mn^{+2}$ and $Mn^{+3}$ occupy the cationic sublattice together with vacancies that assure to keep electro-neutrality condition. To take into account the limited solubility of $ZrO_2$ (up to 4 mol.%) in halite the determined by Pavlyuchkov et al.,[8] $Zr^{+4}$ was introduced into the cationic sublattice and thus the model for halite phase was presented by the formula $(Mg^{+2}, Mn^{+2}, Mn^{+3}, Zr^{+4}, Va)_1(O^{-2})_1$.

The electro-neutrality condition due to the hetero-valent substitution of divalent cation for $Zr^{+4}$ was described by following reaction between end-members:

$$Zr^{+4}O^{-2} + VaO^{-2} = 2 \cdot (Zr_{0.5}Va_{0.5})O \quad \text{(Eq 8)}$$

The Gibbs energy for $VaO^{-2}$ fictive end-member was accepted to be equal to zero in accordance with Kjellqvist and Selleby.[12] The compound $Zr_{0.5}O$ is therefore the fictive end-member with the NaCl structure and its Gibbs energy is equal to ½ (${}^{\circ}G_{ZrO_2\_c} + V3$), where V3 is the parameter to describe the very small solubility of $ZrO_2$ in the halite phase stable in both bounding systems $ZrO_2$-MgO and $ZrO_2$-$MnO_x$. Therefore, the Gibbs energy of the $Zr^{+4}O^{-2}$ fictive compound can be obtained from Eq 6 as follows: ${}^{\circ}G_{Zr+4:O-2} = G_{ZrO_2\_c} + V3 - {}^{\circ}G_{Va:O-2} + 2 \cdot R \cdot T \cdot \ln(2)$, which can be further rearranged to ${}^{\circ}G_{Zr+4:O-2} = G_{ZrO_2\_c} + V3 + 11.52622 \cdot T$.

### 3.4 $ZrO_2$ Based Solid Solutions

The same model described by the formula $(Zr^{+4}, Mg^{+2}, Mn^{+2}, Mn^{+3})_1(O^{-2}, Va)_2$ was applied for all three $ZrO_2$-based solid solutions with the parameters accepted from bounding systems. Additional two ternary parameters describing interaction between $Zr^{+4}$, $Mg^{+2}$, $Mn^{+2}$ and $Zr^{+4}$, $Mg^{+2}$, $Mn^{+3}$ were introduced into c-$ZrO_2$ to describe experimentally determined stability ranges and homogeneity ranges.

Phases present in the system Zr-Mg-Mn-O are listed in Table 1 including crystallographic information and accepted thermodynamic models. It should be mentioned that in the thermodynamic description developed in the present work besides the already mentioned sub-systems like Mn-O, $ZrO_2$-$MnO_x$, $ZrO_2$-MgO and MgO-$MnO_x$, the binary descriptions for the systems of Zr-O,[18] Mg-O,[19] Zr-Mn,[20] Zr-Mg[21] and Mg-Mn[22] were included.

## 4 Optimization Procedure

First of all the thermodynamic description of Grundy et al.[13] was substituted by the thermodynamic description of Kjellqvist and Selleby.[12] It should be noted that this procedure did not substantially influence phase equilibria in sub-solidus region. The liquid phase description was modified by removing $Mn^{+3}$ from the first sublattice and introducing the neutral species $MnO_{1.5}$ to the second sublattice. Correspondently, the mixing parameter in liquid ${}^{0}L(Zr^{+4}, Mn^{+3}:O^{-2})$ was substituted by ${}^{0}L(Zr^{+4}:O^{-2}, MnO_{1.5})$ which was then optimized to reproduce the phase diagram in air and in inert gas atmosphere assuming partial pressure of oxygen equal to 1 × $10^{-4}$ bar.

As mentioned above, introducing $Zr^{+4}$ into the halite and spinel phases should result in some solubility of $ZrO_2$ in halite in the $ZrO_2$-MgO system (spinel should not appear as stable phase in this system) and in $\beta$Sp and halite in the $ZrO_2$-$MnO_x$ system. Solubility of $ZrO_2$ in halite and $\beta$Sp were not modelled in the assessments[8,9] because they were within experimental uncertainty. Therefore, for consistency with experimental data available for the bounding systems the calculated solubility of $ZrO_2$ in these phases should be small.

The next step was the optimization of the end-member parameters in cubic spinel and mixing parameters of the halite phase to reproduce the experimental data[8] for the $ZrO_2$-MgO-$MnO_x$ system. Optimized thermodynamic parameters are presented in Table 2.

## 5 Results and Discussions

The calculated phase diagrams of the $ZrO_2$-MgO and $ZrO_2$-$MnO_x$ systems are presented in Fig. 1(a), (b), (c) and (d) with experimental data.[23–29] The calculations were performed taking into account the gas phase which thermodynamic description was accepted SGTE Substance Database (SGSUB).[30] The calculated data for invariant reactions are compared with the results from previous descriptions[8,9] in Tables 3 and 4. Due to some uncertainty of oxygen partial pressure in inert gas atmosphere[11] calculations in the $ZrO_2$-$MnO_x$ system were performed at oxygen partial pressures equal to 1 × $10^{-4}$ and 3.1 × $10^{-3}$ bar. The phase diagrams only slightly deviate from previous descriptions due to the changes introduced in the present work, but the differences are within experimental uncertainty.

### 5.1 Isothermal Sections of Phase Diagrams of the $ZrO_2$-MgO-$MnO_x$ System

The phase diagrams of the $ZrO_2$-MgO-$MnO_x$ system calculated in the present study at air oxygen partial pressure and fixed temperatures are compared with ones constructed based on experimental data[8] in Fig. 2(a), (b), (c), (d) and (e). It should be noted that isothermal sections in the range between 1523 and 1713 K were reproduced quite well. The stabilization of cubic $ZrO_2$ at temperature of 1613 K, which is below its stability limit in the bounding systems was reproduced by calculations. Phase compositions for equilibrium t-$ZrO_2$ + $\beta$Sp + H at 1523 K and for c-$ZrO_2$ + $\beta$Sp + H at 1613 K were also quite well reproduced by calculations. However, with increasing temperature, the calculations indicated substantial manganese enrichment of halite in the equilibrium c-$ZrO_2$ + $\beta$Sp + H while experiments showed practically the same Mn content in halite at all studied temperatures. As a result, the calculated three-phase equilibrium c-$ZrO_2$ + $\beta$Sp + H was shifted in the Mn rich composition range and is presented by a narrow triangle at temperatures between 1713 and 1913 K. The calculations reproduced the experimentally observed stabilization of the spinel at temperature of 1913 K which was higher than the stability limit of spinel in the MgO-$MnO_x$ system. At 1813 K the calculations showed the formation of spinel at two different composition ranges: first enriched by $MnO_x$ (95-100 mol.% $MnO_x$) and second one at ∼ 40 mol.% of $MnO_x$. According to experimental data 2 mol.% of $ZrO_2$ was enough to stabilize $\beta$-spinel and form a separate phase in the ternary system, while according to calculations the $ZrO_2$ content in $\beta$Sp was substantially higher. It should be also noted that compositions of c-$ZrO_2$ in equilibrium with t-$ZrO_2$ were well reproduced as well as the increase of maximal solubility of stabilizers in c-$ZrO_2$ up to 27 mol.% of MgO and $MnO_x$ together at intermediate compositions. This exceeded the stabilizer solubility in bounding systems $ZrO_2$-MgO and $ZrO_2$-$MnO_x$. Substantial contradictions between calculated and experimental phase equilibria involving liquid phase were observed at 1813 and 1913 K. Calculations indicated two equilibria c-$ZrO_2$ + $\beta$Sp + L and $\beta$Sp + H + L while according to experimental data analysis the stable assemblage involving liquid was c-$ZrO_2$ + H + L at 1813 and 1913 K. Based on the experimental data[8] it was assumed that there were two three-phase equilibria c-$ZrO_2$ + H+$\beta$Sp with minimal and maximal content of $MnO_x$ in $\beta$-spinel. The reason for inconsistency can be limitations in modelling as well as problems of experimental data interpretation due to transformations occurring in samples during cooling.

Phase diagrams calculated at oxygen partial pressures corresponding to protective gas atmosphere ($P(O_2)$ = 1 × $10^{-4}$ bar[8]) and temperatures of 1523 and 1913 K are compared with ones constructed based on experimental data[8] in Fig. 3(a) and (b). The stabilization of c-$ZrO_2$ below its stability ranges in bounding systems was reproduced by calculations at 1523 K though the homogeneity range of c-$ZrO_2$ at these conditions was very narrow and substantially shifted towards the $ZrO_2$-$MnO_x$ bounding system. At 1913 K and $P(O_2)$ = 1 × $10^{-4}$ bar the phase relations were well reproduced indicating melting of c-$ZrO_2$ + H assemblage in the vicinity of the $ZrO_2$-$MnO_x$ bounding system. Calculations at 2003 K and $P(O_2)$ = 1 × $10^{-4}$ bar for composition $ZrO_2$-8.67MgO-61.03$MnO_x$ indicated equilibrium of liquid phase with 16 mol.% of c-$ZrO_2$ phase. This result is consistent with the microstructure investigation of the sample with the above-mentioned composition in protective gas atmosphere

**Table 2** Optimized thermodynamic description for the $ZrO_2$-MgO-$MnO_x$ system (J/mol)

| Phase | Sublattice model | Optimized parameters | Ref. |
|---|---|---|---|
| Ionic liquid | $(Mg^{+2}, Mn^{+2}, Zr^{+4})_P(O^{-2}, MnO_{3/2}, Va)_Q$ | ${}^{\circ}G^{IonicLiquid}_{Mg+2:Va}$ = GMGLIQ | 11 |
| | | ${}^{\circ}G^{IonicLiquid}_{Mg+2:O-2}$ = 2·GMGOLIQ | 11 |
| | | ${}^{\circ}G^{IonicLiquid}_{Mn+2:Va}$ = GLIQMN | 11 |
| | | ${}^{\circ}G^{IonicLiquid}_{Mn+2:O-2}$ = 2·GMNOLIQ | 11 |
| | | ${}^{\circ}G^{IonicLiquid}_{MnO3/2}$ = 0.5·GLMN2O3 | 11 |
| | | ${}^{\circ}G^{IonicLiquid}_{Zr+4:Va}$ = GZRLIQ | 9 |
| | | ${}^{\circ}G^{IonicLiquid}_{Zr+4:O-2}$ = 2·GZRO2LIQ | 9 |
| | | ${}^{\circ}L^{IonicLiquid}_{Mg+2:O-2,Va} = +\ 182000 + 26.8\cdot T$ | 11 |
| | | ${}^{\circ}L^{IonicLiquid}_{Mn+2:O-2,Va} = +\ 129519$ | 11 |
| | | ${}^{1}L^{IonicLiquid}_{Mn+2:O-2,Va} = -\ 45459$ | 11 |
| | | ${}^{\circ}L^{IonicLiquid}_{Mn+2:O-2,MnO3/2} = -\ 33859$ | 11 |
| | | ${}^{\circ}L^{IonicLiquid}_{Mg+2,Mn+2:Va} = +\ 19125 + 12.5\cdot T$ | 11 |
| | | ${}^{\circ}L^{IonicLiquid}_{Mn+2:Va,MnO3/2} = +\ 110000$ | 11 |
| | | ${}^{\circ}L^{IonicLiquid}_{Mg+2:O-2,MnO3/2} = -\ 1110000$ | 11 |
| | | ${}^{\circ}L^{IonicLiquid}_{Mg+2:Va,MnO3/2} = +\ 110000$ | 11 |
| | | ${}^{\circ}L^{IonicLiquid}_{Mg+2,Mn+2:O-2} = +\ 0$ | 11 |
| | | ${}^{\circ}L^{IonicLiquid}_{Mn+2,Zr+4:O-2} = -\ 45000$ | This work |
| | | ${}^{\circ}L^{IonicLiquid}_{Zr+4:O-2,Va} = +\ 75166.0715 - 55.2382004\cdot T$ | 9 |
| | | ${}^{1}L^{IonicLiquid}_{Zr+4:O-2,Va} = +\ 39057.4913$ | 9 |
| | | ${}^{\circ}L^{IonicLiquid}_{Mn+2,Zr+4:Va} = -\ 73668.72 + 30.3\cdot T$ | 10 |
| | | ${}^{1}L^{IonicLiquid}_{Mn+2,Zr+4:Va} = -\ 1991.63$ | 10 |
| | | ${}^{\circ}L^{IonicLiquid}_{Zr+4:O-2,MnO3/2} = +\ 19000$ | This work |
| | | ${}^{\circ}L^{IonicLiquid}_{Mg+2,Zr+4:O-2} = -\ 68195.5443$ | 9 |
| | | ${}^{1}L^{IonicLiquid}_{Mg+2,Zr+4:O-2} = +\ 35835.397$ | 9 |
| | | ${}^{\circ}L^{IonicLiquid}_{Mg+2,Mn+2:Va} = +\ 19125 + 12.5\cdot T$ | 11 |
| | | ${}^{\circ}L^{IonicLiquid}_{Zr+4,Mg+2:Va} = +\ 14003.84 + 29.34205\cdot T$ | 9 |
| Halite | $(Mg^{+2}, Mn^{+2}, Mn^{+3}, Zr^{+4}, Va)_1(O^{-2})_1$ | ${}^{\circ}G^{Halite}_{Mg+2:O-2}$ = GMGOSOL | 11 |
| | | ${}^{\circ}G^{Halite}_{Mn+2:O-2}$ = GMN1O1 | 11 |
| | | ${}^{\circ}G^{Halite}_{Mn+3:O-2} = -\ 21884 + 22.185\cdot T +$ GMN1O1 | This work |
| | | ${}^{\circ}G^{Halite}_{Va:O-2} = +\ 0$ | 11 |
| | | ${}^{\circ}G^{Halite}_{Zr+4:O-2} = +$ GZRO2C $+\ 130000 + 11.5266\cdot T$ | This work |
| | | ${}^{\circ}L^{Halite}_{Mn+2,Mn+3:O-2} = -\ 42105$ | 11 |
| | | ${}^{1}L^{Halite}_{Mn+2,Mn+3:O-2} = +\ 46513$ | 11 |
| | | ${}^{\circ}L^{Halite}_{Mg+2,Mn+2:O-2} = +\ 11000$ | 11 |
| | | ${}^{\circ}L^{Halite}_{Mg+2,Mn+3:O-2} = +\ 50000$ | 11 |
| | | ${}^{\circ}L^{Halite}_{Mg+2,Mn+3,Zr+4:O-2} = +\ 0$ | This work |
| | | ${}^{\circ}L^{Halite}_{Mg+2,Mn+2,Zr+4:O-2} = -\ 200000$ | This work |

**Table 2** continued

| Phase | Sublattice model | Optimized parameters | Ref. |
|---|---|---|---|
| Cubic spinel | $(Mg^{+2}, Mn^{+2})_1(Mg^{+2}, Mn^{+2}, Mn^{+3}, Mn^{+4}, Zr^{+4}, Va)_2(Mg^{+2}, Mn^{+2}, Va)_2(O^{-2})_4$ | $^{\circ}G^{\text{Cubic Spinel}}_{\text{Mg+2:Mg+2:Va:O-2}} = +\ \text{GBMMV}$ | 11 |
| | | $^{\circ}G^{\text{Cubic Spinel}}_{\text{Mn+2:Mn+2:Va:O-2}} = +\ \text{GB22V}$ | 11 |
| | | $T^{\text{Cubic Spinel}}_{\text{CMn+2:Mn+2:Va:O-2}} = 43.1$ | 11 |
| | | $^{\circ}G^{\text{Cubic Spinel}}_{\text{Mn+2:Mn+3:Va:O-2}} = +\ \text{GB23V}$ | 11 |
| | | $T^{\text{Cubic Spinel}}_{\text{CMn+2:Mn+3:Va:O-2}} = 43.1$ | 11 |
| | | $^{\circ}G^{\text{Cubic Spinel}}_{\text{Mn+2:Mn+4:Va:O-2}} = +\ \text{GB24V}$ | 11 |
| | | $T^{\text{Cubic Spinel}}_{\text{CMn+2:Mn+4:Va:O-2}} = 43.1$ | 11 |
| | | $^{\circ}G^{\text{Cubic Spinel}}_{\text{Mg+2:Va:Va:O-2}} = +\ \text{GBMVV}$ | 11 |
| | | $^{\circ}G^{\text{Cubic Spinel}}_{\text{Mn+2:Va:Va:O-2}} = +\ \text{GB2VV}$ | 11 |
| | | $T^{\text{Cubic Spinel}}_{\text{CMn+2:Va:Va:O-2}} = 43.1$ | 11 |
| | | $^{\circ}G^{\text{Cubic Spinel}}_{\text{Mg+2:Mn+4:Va:O-2}} = +\ 4{\cdot}\text{GBM3V} - 2{\cdot}\text{GB23V} - \text{GBMMV} - 60000$ | 11 |
| | | $^{\circ}G^{\text{Cubic Spinel}}_{\text{Mg+2:Mn+2:Va:O-2}} = +\ 2{\cdot}\text{GB23V} + \text{GBMMV} - 2{\cdot}\text{GBM3V} + 60000$ | 11 |
| | | $^{\circ}G^{\text{Cubic Spinel}}_{\text{Mg+2:Mn+3:Va:O-2}} = +\ \text{GBM3V}$ | 11 |
| | | $^{\circ}G^{\text{Cubic Spinel}}_{\text{Mn+2:Mg+2:Va:O-2}} = +\ 2{\cdot}\text{GBM3V} - \text{GB24V}$ | 11 |
| | | $^{\circ}G^{\text{Cubic Spinel}}_{\text{Mg+2:Mg+2:Mg+2:O-2}} = +\ \text{GBMMV} + \text{BADDMG}$ | 11 |
| | | $^{\circ}G^{\text{Cubic Spinel}}_{\text{Mn+2:Mn+2:Mg+2:O-2}} = +\ \text{GB22V} + \text{BADDMG}$ | 11 |
| | | $^{\circ}G^{\text{Cubic Spinel}}_{\text{Mn+2:Mn+3:Mg+2:O-2}} = +\ \text{GB23V} + \text{BADDMG}$ | 11 |
| | | $^{\circ}G^{\text{Cubic Spinel}}_{\text{Mn+2:Mn+4:Mg+2:O-2}} = +\ \text{GB24V} + \text{BADDMG}$ | 11 |
| | | $^{\circ}G^{\text{Cubic Spinel}}_{\text{Mg+2:Va:Mg+2:O-2}} = +\ \text{GBMVV} + \text{BADDMG}$ | 11 |
| | | $^{\circ}G^{\text{Cubic Spinel}}_{\text{Mn+2:Va:Mg+2:O-2}} = +\ \text{GB2VV} + \text{BADDMG}$ | 11 |
| | | $^{\circ}G^{\text{Cubic Spinel}}_{\text{Mg+2:Mn+4:Mg+2:O-2}} = +\ 4{\cdot}\text{GBM3V} - 2{\cdot}\text{GB23V} - \text{GBMMV} - 60000 + \text{BADDMG}$ | 11 |
| | | $^{\circ}G^{\text{Cubic Spinel}}_{\text{Mg+2:Mn+2:Mg+2:O-2}} = +\ 2{\cdot}\text{GB23V} + \text{GBMMV} - 2{\cdot}\text{GBM3V} + 60000 + \text{BADDMG}$ | 11 |
| | | $^{\circ}G^{\text{Cubic Spinel}}_{\text{Mg+2:Mn+3:Mg+2:O-2}} = +\ \text{GBM3V} + \text{BADDMG}$ | 11 |
| | | $^{\circ}G^{\text{Cubic Spinel}}_{\text{Mn+2:Mg+2:Mg+2:O-2}} = +\ 2{\cdot}\text{GBM3V} - \text{GB24V} + \text{BADDMG}$ | 11 |
| | | $^{\circ}G^{\text{Cubic Spinel}}_{\text{Mg+2:Mg+2:Mn+2:O-2}} = +\ \text{GBMMV} + \text{BADDMG} + 100000$ | 11 |
| | | $^{\circ}G^{\text{Cubic Spinel}}_{\text{Mn+2:Mn+2:Mn+2:O-2}} = +\ \text{GB22V} + \text{BADDMG}$ | 11 |
| | | $T^{\text{Cubic Spinel}}_{\text{CMn+2:Mn+2:Mn+2:O-2}} = 43.1$ | 11 |
| | | $^{\circ}G^{\text{Cubic Spinel}}_{\text{Mn+2:Mn+3:Mn+2:O-2}} = +\ \text{GB23V} + \text{BADDMG}$ | 11 |
| | | $T^{\text{Cubic Spinel}}_{\text{CMn+2:Mn+3:Mn+2:O-2}} = 43.1$ | 11 |
| | | $^{\circ}G^{\text{Cubic Spinel}}_{\text{Mn+2:Mn+4:Mn+2:O-2}} = +\ \text{GB24V} + \text{BADDMG}$ | 11 |
| | | $T^{\text{Cubic Spinel}}_{\text{CMn+2:Mn+4:Mn+2:O-2}} = 43.1$ | 11 |
| | | $^{\circ}G^{\text{Cubic Spinel}}_{\text{Mg+2:Va:Mn+2:O-2}} = +\ \text{GBMVV} + \text{BADDMG} + 100000$ | 11 |
| | | $^{\circ}G^{\text{Cubic Spinel}}_{\text{Mn+2:Va:Mn+2:O-2}} = +\ \text{GB2VV} + \text{BADDMG} + 100000$ | 11 |
| | | $T^{\text{Cubic Spinel}}_{\text{CMn+2:Va:Mn+2:O-2}} = 43.1$ | 11 |
| | | $^{\circ}G^{\text{Cubic Spinel}}_{\text{Mg+2:Mn+4:Mn+2:O-2}} = +\ 4{\cdot}\text{GBM3V} - 2{\cdot}\text{GB23V} - \text{GBMMV} + \text{BADDMG} + 40000$ | 11 |
| | | $^{\circ}G^{\text{Cubic Spinel}}_{\text{Mg+2:Mn+2:Mn+2:O-2}} = +\ 2{\cdot}\text{GB23V} + \text{GBMMV} - 2{\cdot}\text{GBM3V} + 160000 + \text{BADDMG}$ | 11 |
| | | $^{\circ}G^{\text{Cubic Spinel}}_{\text{Mg+2:Mn+3:Mn+2:O-2}} = +\ \text{GBM3V} + \text{BADDMG}$ | 11 |
| | | $^{\circ}G^{\text{Cubic Spinel}}_{\text{Mn+2:Mg+2:Mn+2:O-2}} = +\ 2{\cdot}\text{GBM3V} - \text{GB24V} + \text{BADDMG} + 100000$ | 11 |
| | | $^{\circ}G^{\text{Cubic Spinel}}_{\text{Mg+2:Zr+4:Va:O-2}} = +\ \text{GMGZRVA}$ | This work |
| | | $^{\circ}G^{\text{Cubic Spinel}}_{\text{Mn+2:Zr+4:Va:O-2}} = +\ \text{GMNZRVA}$ | This work |
| | | $^{\circ}G^{\text{Cubic Spinel}}_{\text{Mg+2:Zr+4:Mg+2:O-2}} = +\ \text{GMGZRVA} + \text{BADDMG}$ | 9 |

**Table 2** continued

| Phase | Sublattice model | Optimized parameters | Ref. |
|---|---|---|---|
| | | $^{\circ}G^{\text{Cubic Spinel}}_{\text{Mn+2:Zr+4:Mn+2:O-2}}$ = + GMNZRVA + BADDMN | This work |
| | | $^{\circ}G^{\text{Cubic Spinel}}_{\text{Mg+2:Zr+4:Mn+2:O-2}}$ = + GMGZRVA + BADDMN | This work |
| | | $^{\circ}G^{\text{Cubic Spinel}}_{\text{Mn+2:Zr+4:Mg+2:O-2}}$ = + BADDMG + GMNZRVA | This work |
| | | $^{\circ}L^{\text{Cubic Spinel}}_{\text{Mg+2,Mn+2:Zr+4:Va:O-2}}$ = + 766500 − 500·$T$ | This work |
| | | $^{1}L^{\text{Cubic Spinel}}_{\text{Mg+2,Mn+2:Zr+4:Va:O-2}}$ = + 565200 − 400·$T$ | This work |
| c-$ZrO_2$ fluorite | $(Mg^{+2}, Mn^{+2}, Mn^{+3}, Zr^{+4})_1(O^{-2}, Va)_2$ | $^{\circ}G^{\text{C−ZrO2}}_{\text{Mg+2:O-2}}$ = + GMGOSOL + GHSEROO + 45000 + 11.5263·$T$ | 11 |
| | | $^{\circ}G^{\text{C−ZrO2}}_{\text{Mn+2:O-2}}$ = + GMN1O1 + GHSEROO + 45000 + 11.5263·$T$ | 11 |
| | | $^{\circ}G^{\text{C−ZrO2}}_{\text{Mn+3:O-2}}$ = + 0.5·GMN2O3 + 0.5·GHSEROO + 50000 + 9.35108255·$T$ | 11 |
| | | $^{\circ}G^{\text{C−ZrO2}}_{\text{Zr+4:O-2}}$ = + GZRO2C | 9 |
| | | $^{\circ}G^{\text{C−ZrO2}}_{\text{Mg+2:Va}}$ = + GMGOSOL − GHSEROO + 45000 + 11.5263·$T$ | 11 |
| | | $^{\circ}G^{\text{C−ZrO2}}_{\text{Mn+2:Va}}$ = + GMN1O1 − GHSEROO + 45000 + 11.5263·$T$ | 11 |
| | | $^{\circ}G^{\text{C−ZrO2}}_{\text{Mn+3:Va}}$ = + 0.5·GMN2O3 − 1.5·GHSEROO + 50000 + 9.35108255·$T$ | 11 |
| | | $^{\circ}G^{\text{C−ZrO2}}_{\text{Zr+4:Va}}$ = + GZRO2C − 2·GHSEROO | 9 |
| | | $^{\circ}L^{\text{C−ZrO2}}_{\text{Mn+2,Zr+4:*}}$ = − 29547.46 | 10 |
| | | $^{1}L^{\text{C−ZrO2}}_{\text{Mn+2,Zr+4:*}}$ = − 35288.51 | 10 |
| | | $^{\circ}L^{\text{C−ZrO2}}_{\text{Mn+3,Zr+4:*}}$ = − 15461 | 10 |
| | | $^{\circ}L^{\text{C−ZrO2}}_{\text{Mg+2,Zr+4:*}}$ = + 2550.15 | 9 |
| | | $^{\circ}L^{\text{C−ZrO2}}_{\text{Mg+2,Mn+2,Zr+4:*}}$ = − 70000 | This work |
| | | $^{\circ}L^{\text{C−ZrO2}}_{\text{Mg+2,Mn+3,Zr+4:*}}$ = − 20000 | This work |
| t-$ZrO_2$ | $(Mg^{+2}, Mn^{+2}, Mn^{+3}, Zr^{+4})_1(O^{-2}, Va)_2$ | $^{\circ}G^{\text{T−ZrO2}}_{\text{Mg+2:O-2}}$ = + GMGOSOL + GHSEROO + 60000 + 11.5263·$T$ | 9 |
| | | $^{\circ}G^{\text{T−ZrO2}}_{\text{Mn+2:O-2}}$ = + GMN1O1 + GHSEROO + 60000 + 11.5263·$T$ | 10 |
| | | $^{\circ}G^{\text{T−ZrO2}}_{\text{Mn+3:O-2}}$ = + 0.5·GMN2O3 + 0.5·GHSEROO + 50000 + 9.35108255·$T$ | 10 |
| | | $^{\circ}G^{\text{T−ZrO2}}_{\text{Zr+4:O-2}}$ = + GZRO2T | 9 |
| | | $^{\circ}G^{\text{T−ZrO2}}_{\text{Mg+2:Va}}$ = + GMGOSOL − GHSEROO + 60000 + 11.5263·$T$ | 9 |
| | | $^{\circ}G^{\text{T−ZrO2}}_{\text{Mn+2:Va}}$ = + GMN1O1 − GHSEROO + 60000 + 11.5263·$T$ | 10 |
| | | $^{\circ}G^{\text{T−ZrO2}}_{\text{Mn+3:Va}}$ = + 0.5·GMN2O3 − 1.5·GHSEROO + 50000 + 9.35108255·$T$ | 10 |
| | | $^{\circ}G^{\text{T−ZrO2}}_{\text{Zr+4:Va}}$ = + GZRO2T − 2·GHSEROO | 9 |
| | | $^{\circ}L^{\text{T−ZrO2}}_{\text{Mg+2,Zr+4:*}}$ = + 50000 | 9 |
| | | $^{\circ}L^{\text{T−ZrO2}}_{\text{Mn+2,Zr+4:*}}$ = + 44149.358 | 10 |
| | | $^{\circ}L^{\text{T−ZrO2}}_{\text{Mn+3,Zr+4:*}}$ = + 88110.68 | 10 |
| m-$ZrO_2$ | $(Mg^{+2}, Mn^{+2}, Mn^{+3}, Zr^{+4})_1(O^{-2}, Va)_2$ | $^{\circ}G^{\text{M−ZrO2}}_{\text{Mg+2:O-2}}$ = + GMGOSOL + GHSEROO + 120000 + 11.5263·$T$ | 9 |
| | | $^{\circ}G^{\text{M−ZrO2}}_{\text{Mn+2:O-2}}$ = + GMN1O1 + GHSEROO + 120000 + 11.5264·$T$ | 10 |
| | | $^{\circ}G^{\text{M−ZrO2}}_{\text{Mn+3:O-2}}$ = + 0.5·GMN2O3 + 0.5·GHSEROO + 100000 + 9.35108255·$T$ | 10 |
| | | $^{\circ}G^{\text{M−ZrO2}}_{\text{Zr+4:O-2}}$ = + GZRO2M | 9 |
| | | $^{\circ}G^{\text{M−ZrO2}}_{\text{Mg+2:Va}}$ = + GMGOSOL − GHSEROO + 120000 + 11.5263·$T$ | 9 |
| | | $^{\circ}G^{\text{M−ZrO2}}_{\text{Mn+2:Va}}$ = + GMN1O1 − GHSEROO + 11.5263·$T$ + 120000 | 10 |
| | | $^{\circ}G^{\text{M−ZrO2}}_{\text{Mn+3:Va}}$ = + 0.5·GMN2O3 − 1.5·GHSEROO + 9.35108255·$T$ + 100000 | 10 |
| | | $^{\circ}G^{\text{M−ZrO2}}_{\text{Zr+4:Va}}$ = + GZRO2M − 2·GHSEROO | 9 |
| Functions | (Temperature limits) | | |
| GHSEROO | (298-1000) | − 3480.87 − 25.503038•$T$ − 11.136•$T$•LN($T$) − 0.005098888•$T^2$ + 6.61846 × $10^{-7}$ $T^3$ − 38365•$T^{-1}$ | |
| | (1000-3300) | − 6568.763 + 12.65988•$T$ − 16.8138•$T$•LN($T$) − 5.95798 × $10^{-4}$•$T^2$ + 6.781 × $10^{-9}$•$T^3$ + 262905•$T^{-1}$ | |

**Table 2** continued

| Phase | Sublattice model | Optimized parameters | Ref. |
|---|---|---|---|
| | (3300-6000) | $-13986.728 + 31.259625\bullet T - 18.9536\bullet T\bullet \mathrm{LN}(T) - 4.25243\times 10^{-4}\bullet T^2 + 1.0721\times 10^{-8}\bullet T^3 + 4383200\bullet T^{-1}$ | |
| GHSERMG | (298-923) | $-8367.34 + 143.677875\bullet T - 26.1849782\bullet T\bullet \mathrm{LN}(T) + 4.858\times 10^{-4}\bullet T^2 - 1.393669\times 10^{-6}\bullet T^3 + 78950\bullet T^{-1}$ | |
| | (923-3000) | $-14130.185 + 204.718543\bullet T - 34.3088\bullet T\bullet \mathrm{LN}(T) + 1.038192\bullet 10^{+28}\bullet T^{-9}$ | |
| GMGLIQ | (298-923) | $+8202.243 - 8.83693\bullet T + \mathrm{GHSERMG} - 8.0176\times 10^{-20}\bullet T^7$ | |
| | (923-3000) | $+8690.316 - 9.392158\bullet T + \mathrm{GHSERMG} - 1.038192\bullet 10^{+28}\bullet T^{-9}$ | |
| GMGOSOL | (298-1700) | $-619428.502 + 298.253571\bullet T - 47.4817\bullet T\bullet \mathrm{LN}(T) - 0.00232681\bullet T^2 + 4.5043\times 10^{-8}\bullet T^3 + 516900\bullet T^{-1}$ | |
| | (1700-3100) | $-655489.818 + 528.597187\bullet T - 78.3772\bullet T\bullet \mathrm{LN}(T) + 0.0097344\bullet T^2 - 8.60338\times 10^{-7}\bullet T^3 + 8591550\bullet T^{-1}$ | |
| | (3100-5000) | $-171490.159 - 1409.43369\bullet T + 163.674142\bullet T\bullet \mathrm{LN}(T) - 0.044009535\bullet T^2 + 1.374896\times 10^{-6}\bullet T^3 - 1.72665403\bullet 10^{+8}\bullet T^{-1}$ | |
| | (5000-5100) | $-722412.718 + 617.657452\bullet T - 84\bullet T\bullet \mathrm{LN}(T)$ | |
| GMGOLIQ | (298-1700) | $-549098.33 + 275.724634\bullet T - 47.4817\bullet T\bullet \mathrm{LN}(T) - 0.00232681\bullet T^2 + 4.5043\times 10^{-8}\bullet T^3 + 516900\bullet T^{-1}$ | |
| | (1700-2450) | $-585159.646 + 506.06825\bullet T - 78.3772\bullet T\bullet \mathrm{LN}(T) + 0.0097344\bullet T^2 - 8.60338\times 10^{-7}\bullet T^3 + 8591550\bullet T^{-1}$ | |
| | (2450-3100) | $+9110429.75 - 42013.7634\bullet T + 5298.548\bullet T\bullet \mathrm{LN}(T) - 1.30122485\bullet T^2 + 5.8262601\times 10^{-5}\bullet T^3 - 3.24037416\bullet 10^{9}\bullet T^{-1}$ | |
| | (3100-5100) | $-632664.468 + 589.239555\bullet T - 84\bullet T\bullet \mathrm{LN}(T)$ | |
| GLIQMN | (298-1519) | $+17859.91 - 12.6208\bullet T + \mathrm{GHSERMN} - 4.41929\times 10^{-21}\bullet T^7$ | |
| | (1519-2000) | $-9993.9 + 299.036*T - 48*T*\mathrm{LN}(T)$ | |
| GMN1O1 | (298-6000) | $-402478 + 259.356\bullet T - 46.835\bullet T\bullet \mathrm{LN}(T) - 0.00385\bullet T^2 + 212922\bullet T^{-1}$ | |
| GMNOLIQ | (298-6000) | $+\mathrm{GMN1O1} + 43947 - 20.628\bullet T$ | |
| GMN2O3 | (298-6000) | $-998618 + 588.619\bullet T - 101.956\bullet T\bullet \mathrm{LN}(T) - 0.018844\bullet T^2 + 589055\bullet T^{-1}$ | |
| GLMN2O3 | (298-6000) | $+2\bullet \mathrm{GMN1O1} + \mathrm{GHSEROO} - 64953 + 43.144\bullet T$ | |
| GAMN3O4 | (298-6000) | $-1439700 + 892.2\bullet T - 154.748\bullet T\bullet \mathrm{LN}(T) - 0.017408\bullet T^2 + 986139\bullet T^{-1}$ | |
| GMN3O4B | (298-6000) | $+15270 + 7\bullet T$ | |
| GMNFE2O4 | (298-6000) | $-182450 + 133\bullet T - 23.099\bullet T\bullet \mathrm{LN}(T) - 0.0014\bullet T^2 + 124000\bullet T^{-1}$ | |
| GHSERZR | (130-2128) | $-7827.595 + 125.64905\bullet T - 24.1618\bullet T\bullet \mathrm{LN}(T) - 0.00437791\bullet T^2 + 34971\bullet T^{-1}$ | |
| | (2128-6000) | $-26085.921 + 262.724183\bullet T - 42.144\bullet T\bullet \mathrm{LN}(T) - 1.342896\bullet 10^{31}\bullet T^{-9}$ | |
| GZRLIQ | (130-2128) | $+18147.69 - 9.080812\bullet T + \mathrm{GHSERZR} + 1.6275\times 10^{-22}\bullet T^7$ | |
| | (2128-6000) | $-8281.26 + 253.812609\bullet T - 42.144\bullet T\bullet \mathrm{LN}(T)$ | |
| GZRO2M | (298-6000) | $-1126163.54 + 424.890806\bullet T - 69.3875137\bullet T\bullet \mathrm{LN}(T) - 0.00375880141\bullet T^2 + 683000\bullet T^{-1}$ | |
| GZRO2*T* | (298-6000) | $+5468 - 4\bullet T + \mathrm{GZRO2M}$ | |
| GZRO2C | (298-6000) | $+10336 - 4\bullet T + \mathrm{GZRO2}T$ | |
| GZRO2LIQ | (298-6000) | $+87027 - 29.17432\bullet T + \mathrm{GZRO2C}$ | |
| NCUBIC SPINEL | (298-6000) | $+\mathrm{GMGOSOL} + \mathrm{GCORUND} - 27600 - 62\bullet T + 9\bullet T\bullet \mathrm{LN}(T)$ | |
| ICUBIC SPINEL | (298-6000) | $+\mathrm{NCUBIC\ SPINEL} + 51600 - 39\bullet T$ | |
| GCORUND | (298-600) | $-1707351.3 + 448.021092\bullet T - 67.4804\bullet T\bullet \mathrm{LN}(T) - 0.06747\bullet T^2 + 1.4205433\times 10^{-5}\bullet T^3 + 938780\bullet T^{-1}$ | |
| | (600-1500) | $-1724886.06 + 754.856573\bullet T - 116.258\bullet T\bullet \mathrm{LN}(T) - 0.0072257\bullet T^2 + 2.78532\times 10^{-7}\bullet T^3 + 2120700\bullet T^{-1}$ | |
| | (1500-3000) | $-1772163.19 + 1053.4548\bullet T - 156.058\bullet T\bullet \mathrm{LN}(T) + 0.00709105\bullet T^2 - 6.29402\times 10^{-7}\bullet T^3 + 12366650\bullet T^{-1}$ | |
| GGAMMA | (298-600) | $-1689977.34 + 469.458181\bullet T - 70.5452\bullet T\bullet \mathrm{LN}(T) - 0.070794\bullet T^2 + 1.491345\times 10^{-5}\bullet T^3 + 981165\bullet T^{-1}$ | |
| | (600-1500) | $-1708389.72 + 791.591946\bullet T - 121.754\bullet T\bullet \mathrm{LN}(T) - 0.0075467\bullet T^2 + 2.89573\times 10^{-7}\bullet T^3 + 2222750\bullet T^{-1}$ | |
| | (1500-3000) | $-1758861.74 + 1110.41976\bullet T - 164.253\bullet T\bullet \mathrm{LN}(T) + 0.00775305\bullet T^2 - 6.8247\times 10^{-7}\bullet T^3 + 13162750\bullet T^{-1}$ | |
| NSPFEAL | (298-6000) | $-287500 + 136\bullet T - 22.1991\bullet T\bullet \mathrm{LN}(T) - 0.001867857\bullet T^2 + 223844\bullet T^{-1}$ | |

**Table 2** continued

| Phase | Sublattice model | Optimized parameters | Ref. |
|---|---|---|---|
| BFE3O4 | (298-3000) | + 46826 − 27.266•$T$ | |
| GFE3O4 | (298-3000) | − 161731 + 144.873•$T$ − 24.9879•$T$•LN($T$) − 0.0011952256•$T^2$ + 206520•$T^{-1}$ | |
| G22V | (298-6000) | + 7•GFE3O4 + BFE3O4 | |
| G2AV | (298-6000) | + 7•NSPFEAL | |
| GB_JK | (298-6000) | + 0.142857143•GAMN3O4 + 0.142857143•GMN3O4B | |
| KMN3O4B | (298-6000) | + 26210 − 17.46•$T$ | |
| REFSPAAV | (298-6000) | + 1.5•G2AV − 0.5•G22V + 32900 | |
| GGMN2O3B | (298-6000) | + GMN2O3 + 192300 − 193.8•$T$ + 0.05•$T^2$ | |
| MCUBIC SPINEL | (298-6000) | + GMGOSOL + 58000 − 18•$T$ | |
| BADDMG | (298-6000) | + 8•MCUBIC SPINEL − 2•NCUBIC SPINEL − 4•ICUBIC SPINEL − 23.0527167 + 4•REFSPAAV | |
| GMGZRVA | (298-6000) | + 4•GMGOSOL + 2•GZRO2C + 30000 + 23.05244•$T$ − GBMMV (*this work*) | |
| GMNZRVA | (298-6000) | + 4•GMN1O1 + 2•GZRO2C + 70000 + 23.05244•$T$ − GB22V (*this work*) | |
| GMN2MGO4 | (298-6000) | − 1629500 + 983.45•$T$ − 166.1•$T$•LN($T$) + 2.97 × $10^{-4}$•$T^2$ + 1470000•$T^{-1}$ | |
| GBMMV | (298-6000) | + NCUBIC SPINEL + 2•ICUBIC SPINEL + 23.0527167•$T$ − 2•REFSPAAV• | |
| GB22V | (298-6000) | + 21•GMNFE2O4 + 56000 − 14•GFE3O4 + 2•BFE3O4 | |
| GB23V | (298-6000) | + 7•GB_JK | |
| GB24V | (298-6000) | + 14•GB_JK − 21•GMNFE2O4 − 56000 + 14•GFE3O4 − 2•BFE3O4 + KMN3O4B | |
| GBMVV | (298-6000) | + 8•GGAMMA + NCUBIC SPINEL + 44.9543481•$T$ + 108000 − 6•REFSPAAV | |
| GB2VV | (298-6000) | + 8•GGMN2O3B − 56•GB_JK + 63•GMNFE2O4 + 168000 − 42•GFE3O4 + 6•BFE3O4 − 3•KMN3O4B + 12•R•$T$•LN(6) − 6•R•$T$•LN(3) − 4•R•$T$•LN(2) | |
| GBM3V | (298-6000) | + GMN2MGO4 + 52000 − 18•$T$ | |

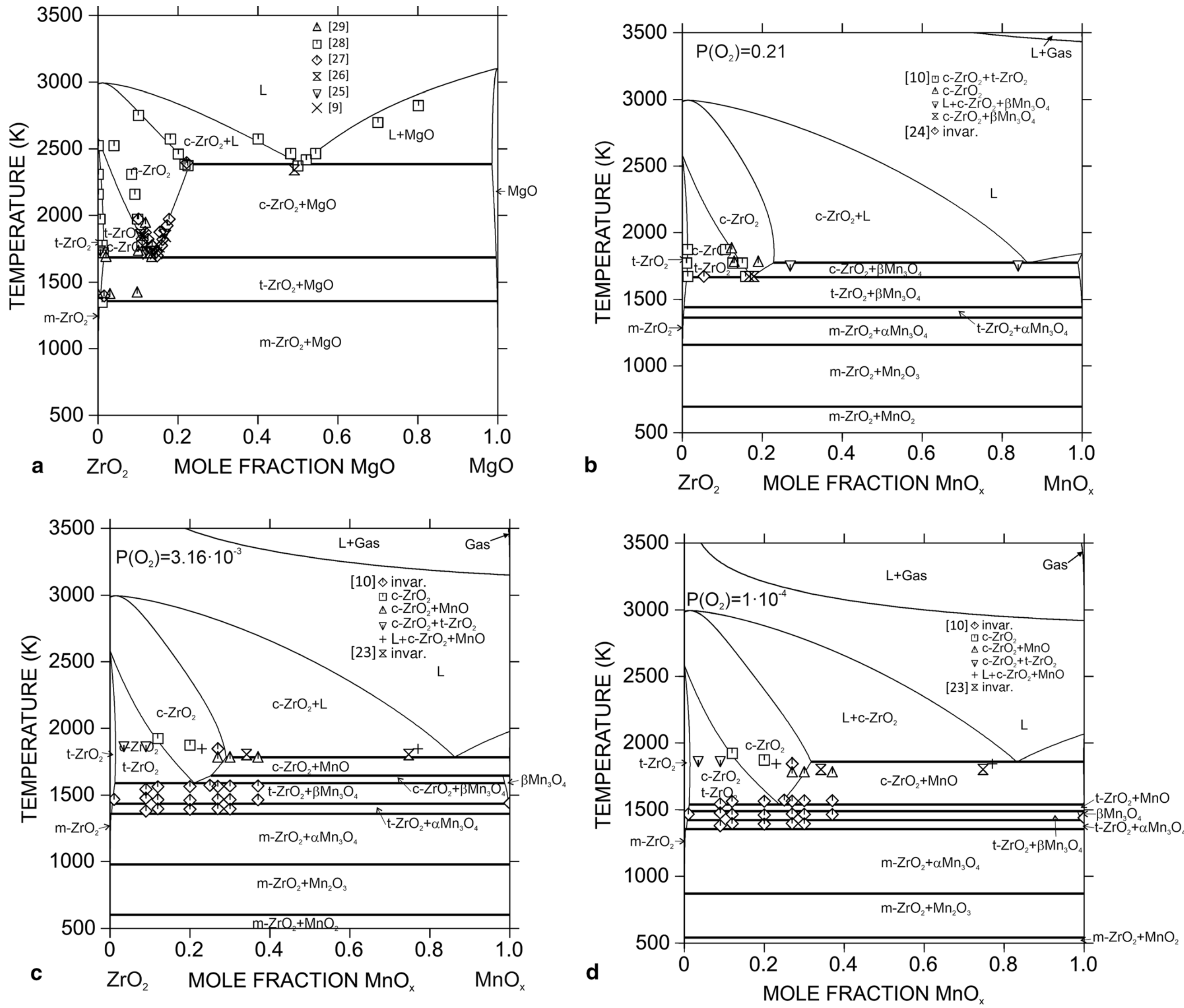


**Fig. 1** Calculated phase diagrams for (a) the $ZrO_2$-MgO system; (b) the $ZrO_2$-$MnO_x$ system in air; (c) the $ZrO_2$-$MnO_x$ system at $P(O_2) = 3.16 \times 10^{-3}$; (d) the $ZrO_2$-$MnO_x$ system at $P(O_2) = 1 \times 10^{-4}$

indicating small amount of primary c-$ZrO_2$ along with a wide eutectic area (Fig. 4).

## 5.2 Experimental Investigations

Two samples with compositions $ZrO_2$-8.67MgO-61.03$MnO_x$ and $ZrO_2$-58.33MgO-16.08$MnO_x$ (in mol.%) after preliminary heat treatment in He atmosphere were investigated using DTA. The DTA-TG heating curves are presented in Fig. 5(a) and (b) together with calculated phase fraction diagrams. Though there were some inconsistencies between calculated and experimental phase diagrams, as discussed above the calculations help to interpret the obtained DTA results. It should be noted that there was an overheating effect for the m-$ZrO_2$ to t-$ZrO_2$ transformation indicated in pure $ZrO_2$[31] as well as in the solid solutions.[9]

It should be noted that XRD indicated the presence of halite and cubic $ZrO_2$ in both samples after heat treatment at 1913 K. In both samples exothermic effects were observed at 991 K, indicating the transformations of the initial phase assemblage c-$ZrO_2$ + H into the stable assemblage.

According to calculations the stable assemblage for the sample of $ZrO_2$-8.67MgO-61.03$MnO_x$ (in mol.%) composition at 1000 K should be αSp + m-$ZrO_2$. The first heat effect at 1201 K can be related to the appearance of the halite phase observed in the calculated phase fraction diagram at 1250 K. The formation of halite should be associated with a small mass loss since only a small

**Table 3** Calculated and experimental data on invariant reactions in the $ZrO_2$-MgO system

| Reaction, mol.% MgO | | | | | Type | $T$ (K) | References |
|---|---|---|---|---|---|---|---|
| L | ↔ | c-$ZrO_2$ | + | MgO | Eutectic | | |
| 50.78 | | 22.90 | | 98.51 | | 2384 | This work |
| 51.29 | | 23.17 | | 100 | | 2376 | 9 |
| c-$ZrO_2$ | ↔ | t-$ZrO_2$ | + | MgO | Eutectoid | | |
| 13.68 | | 1.47 | | 99.58 | | 1685 | This work |
| 13.71 | | 1.47 | | 100 | | 1683 | 9 |
| t-$ZrO_2$ | ↔ | m-$ZrO_2$ | + | MgO | Eutectoid | | |
| 0.55 | | 0.34 | | 99.87 | | 1356 | This work |
| 0.55 | | 0.35 | | 100 | | 1356 | 9 |

**Table 4** Calculated and experimental data on invariant reactions in the $ZrO_2$-$MnO_x$ system

| Reaction, 100Mn/(Mn + Zr), mol.% | | | | | Type | T (K) | References |
|---|---|---|---|---|---|---|---|
| P($O_2$) = 0.21 bar | | | | | | | |
| L | ↔ | c-$ZrO_2$ | + | βSp | Eutectic | | |
| 86.38 | | 22.83 | | 98.92 | | 1775 | This work |
| 86.5 | | 23.5 | | 100 | | 1786 | 10 |
| c-$ZrO_2$ | ↔ | t-$ZrO_2$ | + | βSp | Eutectoid | | |
| 17.40 | | 1.17 | | 99.40 | | 1668 | This work |
| 17.4 | | 1.15 | | 100 | | 1669 | 10 |
| βSp | ↔ | t-$ZrO_2$ | + | αSp | Eutectoid | | |
| 99.91 | | 0.44 | | 100 | | 1441 | This work |
| … | | … | | … | | 1443 | 10 |
| t-$ZrO_2$ | ↔ | m-$ZrO_2$ | + | αSp | Eutectoid | | |
| 0.55 | | 0.34 | | 100 | | 1363 | This work |
| … | | … | | … | | 1362 | 10 |
| αSp | ↔ | $Mn_2O_3$ | + | m-$ZrO_2$ | Degenerated | | |
| 100 | | 100 | | 0.08 | | 1159 | This work |
| … | | … | | … | | 1133 | 10 |
| $Mn_2O_3$ | ↔ | $MnO_2$ | + | m-$ZrO_2$ | Degenerated | | |
| 100 | | 100 | | 0 | | 694 | This work |
| P($O_2$) = 3.16 × $10^{-3}$ bar | | | | | | | |
| L | ↔ | c-$ZrO_2$ | + | H | Eutectic | | |
| 86.24 | | 29.04 | | 99.95 | | 1782 | This work |
| c-$ZrO_2$ | + | H | ↔ | βSp | Peritectoid | | |
| 25.26 | | 99.98 | | 98.23 | | 1645 | This work |
| c-$ZrO_2$ | ↔ | t-$ZrO_2$ | + | βSp | Eutectoid | | |
| 21.05 | | 1.22 | | 98.71 | | 1590 | This work |
| βSp | ↔ | t-$ZrO_2$ | + | αSp | Eutectoid | | |
| 99.67 | | 0.60 | | 100 | | 1434 | This work |
| t-$ZrO_2$ | ↔ | m-$ZrO_2$ | + | αSp | Eutectoid | | |
| 0.40 | | 0.25 | | 100 | | 1358 | This work |
| αSp | ↔ | $Mn_2O_3$ | + | m-$ZrO_2$ | Degenerated | | |
| 100 | | 100 | | 0.02 | | 978 | This work |
| $Mn_2O_3$ | ↔ | $MnO_2$ | + | m-$ZrO_2$ | Degenerated | | |
| 100 | | 100 | | 0 | | 600 | This work |

**Table 4** continued

| Reaction, 100Mn/(Mn + Zr), mol.% | | | | | Type | T (K) | References |
|---|---|---|---|---|---|---|---|
| $P(O_2) = 1 \times 10^{-4}$ bar | | | | | | | |
| L | ↔ | $c\text{-}ZrO_2$ | + | H | Eutectic | | |
| 83.15 | | 31.72 | | 99.81 | | 1860 | This work |
| 80.00 | | 30.6 | | 100 | | 1805 | 10 |
| $c\text{-}ZrO_2$ | ↔ | $t\text{-}ZrO_2$ | + | H | Eutectoid | | |
| 23.76 | | 1.22 | | 99.98 | | 1540 | This work |
| 23.80 | | 1.20 | | 100 | | 1540 | 10 |
| $t\text{-}ZrO_2$ | + | H | ↔ | $\beta$Sp | Peritectoid | | |
| 1.05 | | 99.99 | | 98.33 | | 1488 | This work |
| … | | … | | … | | 1487 | 10 |
| $\beta$Sp | ↔ | $\alpha$Sp | + | $t\text{-}ZrO_2$ | Eutectoid | | |
| 99.11 | | 100 | | 0.75 | | 1421 | This work |
| 100 | | 100 | | 1.00 | | 1443 | 10 |
| $t\text{-}ZrO_2$ | ↔ | $\alpha$Sp | + | $m\text{-}ZrO_2$ | Eutectoid | | |
| 0.52 | | 100 | | 0.29 | | 1354 | This work |
| 0.52 | | 100 | | 0.30 | | 1354 | 10 |
| $\alpha$Sp | ↔ | $Mn_2O_3$ | + | $m\text{-}ZrO_2$ | Degenerated | | |
| 100 | | 100 | | 0 | | 869 | This work |
| $Mn_2O_3$ | ↔ | $MnO_2$ | + | $m\text{-}ZrO_2$ | Degenerated | | |
| 100 | | 100 | | 0 | | 540 | This work |

fraction ~ 8 mol.% of halite phase should be formed according to the calculations. The effect observed at 1315 K can be related to the transformation of $\alpha$Sp into $\beta$Sp. The next effect at 1481 K can be related to the transformation of $m\text{-}ZrO_2$ into $t\text{-}ZrO_2$. It should be noted that according to the calculations both transformations occurred at approximately the same temperature of 1350 K. As it was mentioned above monoclinic to tetragonal phase transformation usually occurs with a large overheating effect exceeding 100 K. The effect at 1544 K can be explained by the disappearance of $\beta$Sp due to its transformation to the halite phase accompanied with mass loss which can be observed on the TG curve. According to the calculations this transformation occurs at 1460 K. The effect at 1624 K can be related to the transformation of $t\text{-}ZrO_2$ into $c\text{-}ZrO_2$ which can dissolve more stabilizer than $t\text{-}ZrO_2$. Therefore, the amount of halite phase should slightly decrease. The calculated temperature of the $t\text{-}ZrO_2$ to $c\text{-}ZrO_2$ transformation is 1525 K. The observed difference can be caused by an overheating effect due to kinetic reasons. The last effect at 1903 K can be explained by the melting of the $c\text{-}ZrO_2$ + H assemblage. This is in perfect agreement with the calculations, that indicates the beginning of melting at 1890 K. The shape of the peak indicates that there are two transformations. The calculations show that during melting the halite phase disappears at 1920 K. Therefore, the second effect in the melting peak can be related to the disappearance of halite.

The calculated stable assemblage for the sample with composition $ZrO_2$-58.33MgO-16.08$MnO_x$ (in mol.%) at 1000 K should be H + $\alpha$Sp + $m\text{-}ZrO_2$. The first effect in the heating curve was observed at 1214 K. It can be related to the transformation of $\alpha$Sp into the halite phase accompanied by mass loss. The mass loss was confirmed by the TG heating curve. The calculations show that a sharp decrease of $\alpha$Sp content starts at ~ 1200 K and finishes at 1300 K. However, in DTA this process occurs with some overheating due to kinetic reasons and finishes at substantially higher temperatures. Besides this there was an uncertainty concerning the oxygen partial pressure in the DTA. Calculations showed that if the partial pressure was $3.2 \times 10^{-3}$ bar as assumed by Dilner et al.[11] the stable phase will be $\beta$Sp and it will disappear at higher temperatures. Next two heat effects at 1398 and 1575 K can be related to transformation of $m\text{-}ZrO_2$ to $t\text{-}ZrO_2$ which further transforms into $c\text{-}ZrO_2$. According to the calculations these transformations occurred at 1350 and 1589 K, respectively. The last transformation occurs in some temperature range until all $t\text{-}ZrO_2$ is transformed into $c\text{-}ZrO_2$ at 1594 K. It should be noted that according to the calculations the $t\text{-}ZrO_2$ dissolves a small amount of stabilizer (MnO + MgO), while $c\text{-}ZrO_2$ dissolved up to 25 mol.% of

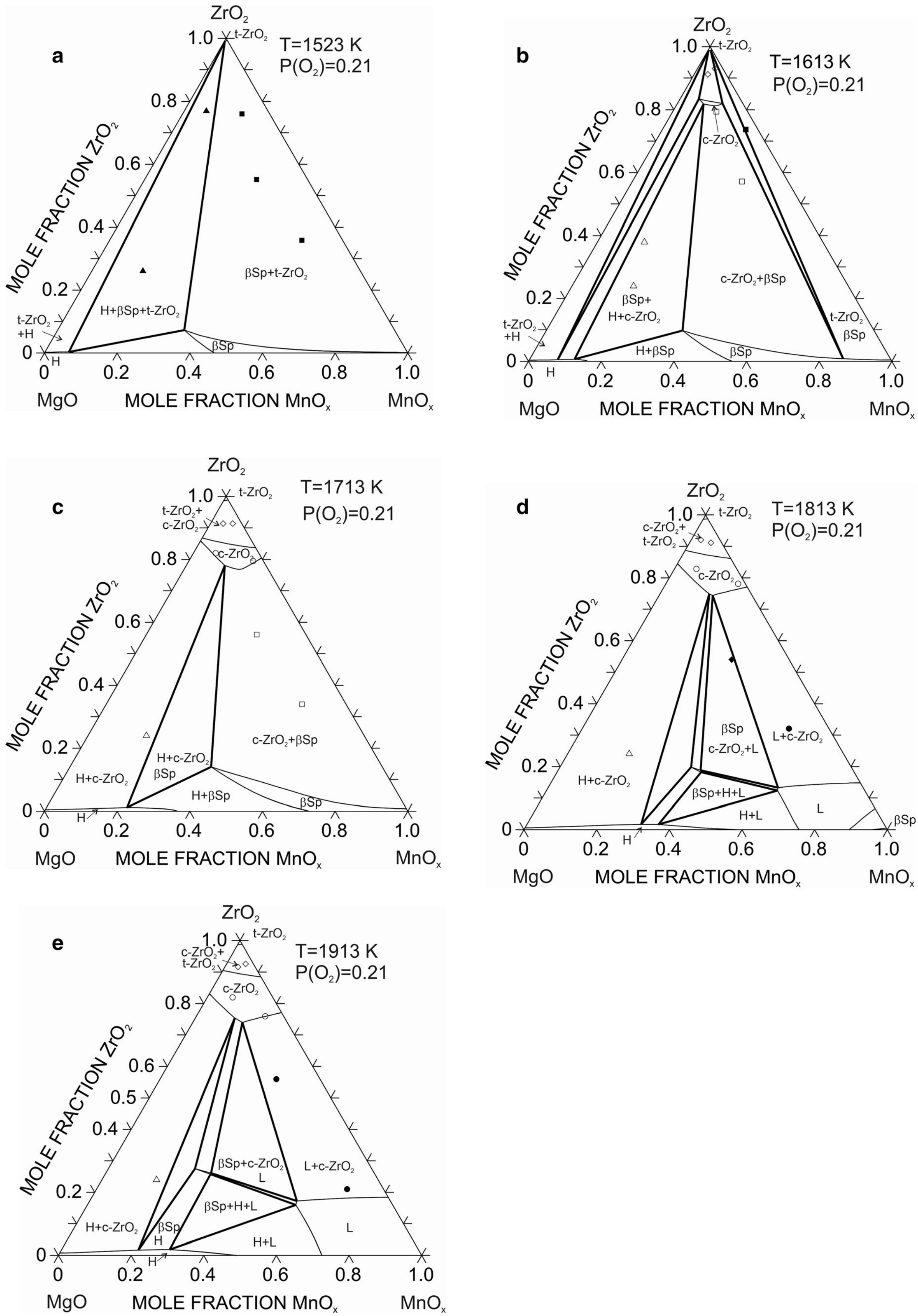
a
ZrO2
t-ZrO2
T=1523 K
P(O2)=0.21
MOLE FRACTION ZrO2
βSp+t-ZrO2
H+βSp+t-ZrO2
t-ZrO2 +H
βSp
H
MgO
MOLE FRACTION MnOx
MnOx
b
T=1613 K
P(O2)=0.21
c-ZrO2
c-ZrO2+βSp
βSp+ H+c-ZrO2
t-ZrO2 βSp
H+βSp
βSp
c
T=1713 K
P(O2)=0.21
t-ZrO2+ c-ZrO2
c-ZrO2
c-ZrO2+βSp
H+c-ZrO2 βSp
H+c-ZrO2
H+βSp
βSp
d
T=1813 K
P(O2)=0.21
c-ZrO2+ t-ZrO2
βSp c-ZrO2+L
L+c-ZrO2
βSp+H+L
H+L
L
e
T=1913 K
βSp+c-ZrO2 L
L+c-ZrO2
βSp+H+L
H+L
βSp H
0 0.2 0.4 0.6 0.8 1.0

◀**Fig. 2** Calculated isothermal sections of the $ZrO_2$-MgO-$MnO_x$ system at: (a) 1523; (b) 1613 K; (c) 1713 K; (d) 1813 K; (e) 1913 K in air with experimental data from Pavlyuchkov et al.[8] Open circles—c-$ZrO_2$; closed circles—c-$ZrO_2$ + H + L; closed rectangles—t-$ZrO_2$ + βSp; open rectangles—c-$ZrO_2$ + βSp; closed triangles—t-$ZrO_2$ + βSp + H; open triangles—c-$ZrO_2$ + βSp + H; open rhombuses—t-$ZrO_2$ + c-$ZrO_2$; closed rhombuses—c-$ZrO_2$ + H

stabilizer that is also consistent with the experimental data of Pavlyuchkov et al.[8] Therefore, the amount of halite phase decreases due to the dissolution of MgO and MnO in c-$ZrO_2$. According to the calculation the dissolution of MgO and MnO occurs simultaneously with formation of c-$ZrO_2$. However, in the DTA this process is substantially slower and finish at 1863 K which can be observed as the last heat effect on the heating curve.

Calculated mass loss for both compositions $ZrO_2$-8.67MgO-61.03$MnO_x$ and $ZrO_2$-58.33MgO-16.08$MnO_x$ (in mol.%) are compared with TG data in Fig. 6(a) and (b). In calculations, components were selected as MgO, MnO and $O_2$. Mass% of $O_2$ presented at the plots show the difference in mass between halite and spinel. Calculated mass loss is in reasonable agreement with TG though the temperature of the beginning and end of mass loss show deviation from experimental data. The reason for these inconsistencies can be explained by the fact that the partial pressure of oxygen was not controlled in the experiments and by influence of kinetics from one side and uncertainty of calculations from another side. It should be noted that calculations show some small mass gain due to higher concentration of $Mn^{+3}$ in $\beta$Sp and in liquid. However, it is not clear if such effects can be observed in DTA/TG experiments.

Though the experiments have some uncertainties, such as oxygen partial pressure and kinetic effects, the derived thermodynamic description helps to relate observed heat effects with phase transformations and chemical reactions.

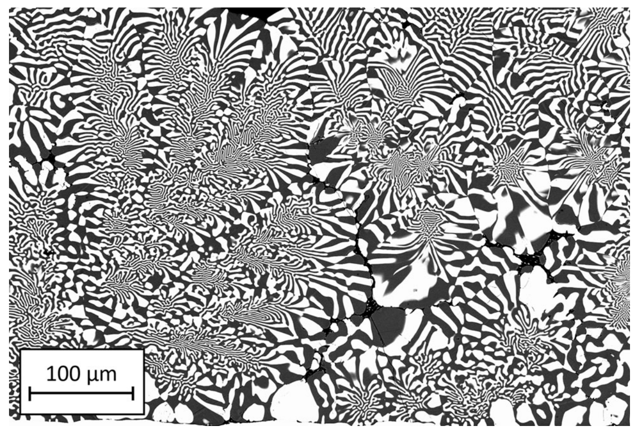


**Fig. 4** Microstructure of the sample $ZrO_2$-8.67MgO-61.03$MnO_x$ annealed at 1913 K during 15 min in He atmosphere (light phase—c-$ZrO_2$, dark grey phase—Halite)

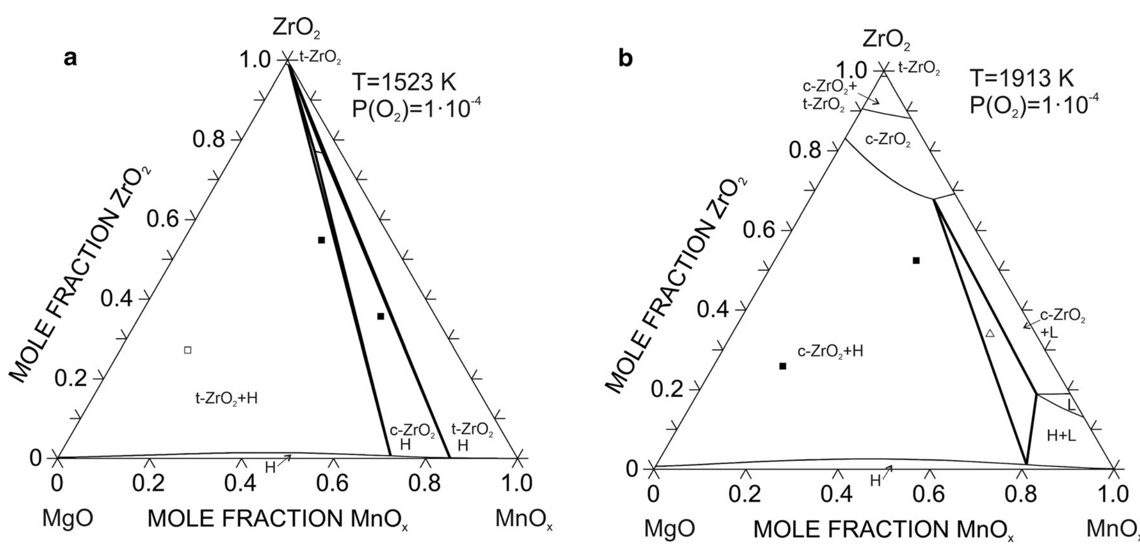


**Fig. 3** Calculated isothermal sections of the $ZrO_2$-MgO-$MnO_x$ system at oxygen partial pressure corresponding protective gas atmosphere ($P(O_2) = 1 \times 10^{-4}$ bar) at: (a) 1523; (b) 1913 K with experimental data from Pavlyuchkov et al.[8] Closed rectangles—c-$ZrO_2$ + H; open rectangles—t-$ZrO_2$ + H; open triangles—c-$ZrO_2$ + H + L

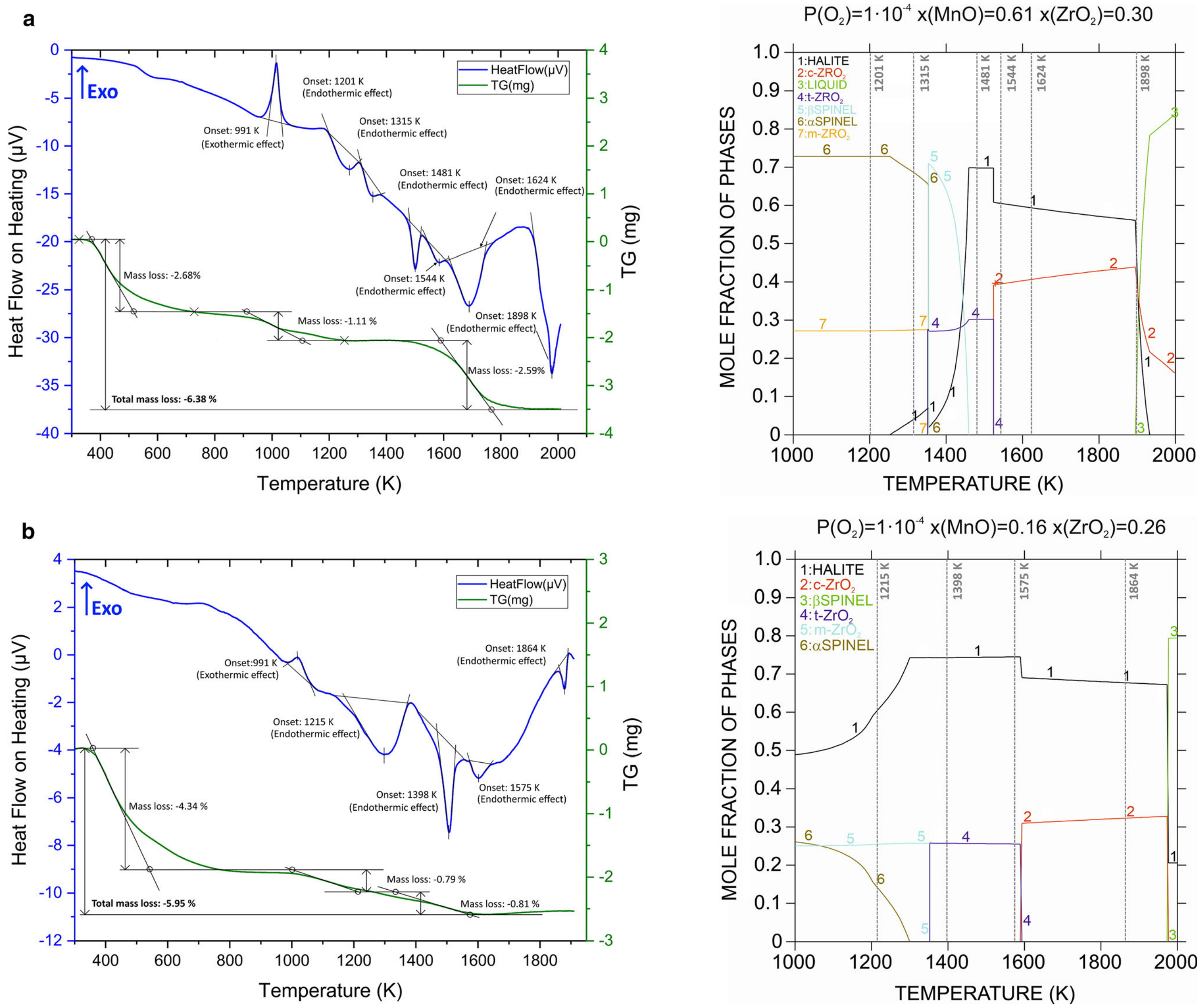


**Fig. 5** DTA-TG data in comparison with calculated phase fraction diagrams for compositions: (a) $ZrO_2$-8.67MgO-61.03$MnO_x$ and (b) $ZrO_2$-58.33MgO-16.08$MnO_x$ (in mol.%). Grey lines in the phase fraction diagrams label onset points of DTA results

## 6 Conclusions

A thermodynamic database for the $ZrO_2$-MgO-$MnO_x$ system was derived based on experimental data of Pavlyuchkov et al.[8] Thermodynamic modelling of the current oxide system has been performed for the first time. This work focused on the reproduction of the phase diagrams for oxide systems. The main features described are the stabilization of cubic $ZrO_2$ based solid solutions at temperatures below their stability limits in the bounding systems both in air and protective gas atmosphere as well as stabilization of cubic spinel ($\beta$Sp) at temperatures above its stability limits in bounding systems. The thermodynamic description also incorporates all available descriptions of the binary subsystems. The obtained thermodynamic description was verified by interpretation of DTA-TG results obtained for two samples with compositions $ZrO_2$-8.67MgO-61.03$MnO_x$ and $ZrO_2$-58.33MgO-16.08$MnO_x$ (in mol.%). Calculated phase fraction diagrams were used to interpret observed heat effects and mass loses.

The current database can be used for further thermodynamic modelling of the high-order systems for the development of the TRIP-Matrix-Composites.[3,32] Thus, results of current modelling can be applied for optimization of the coating process of the Mg-PSZ mentioned above. Moreover, the obtained thermodynamic description has

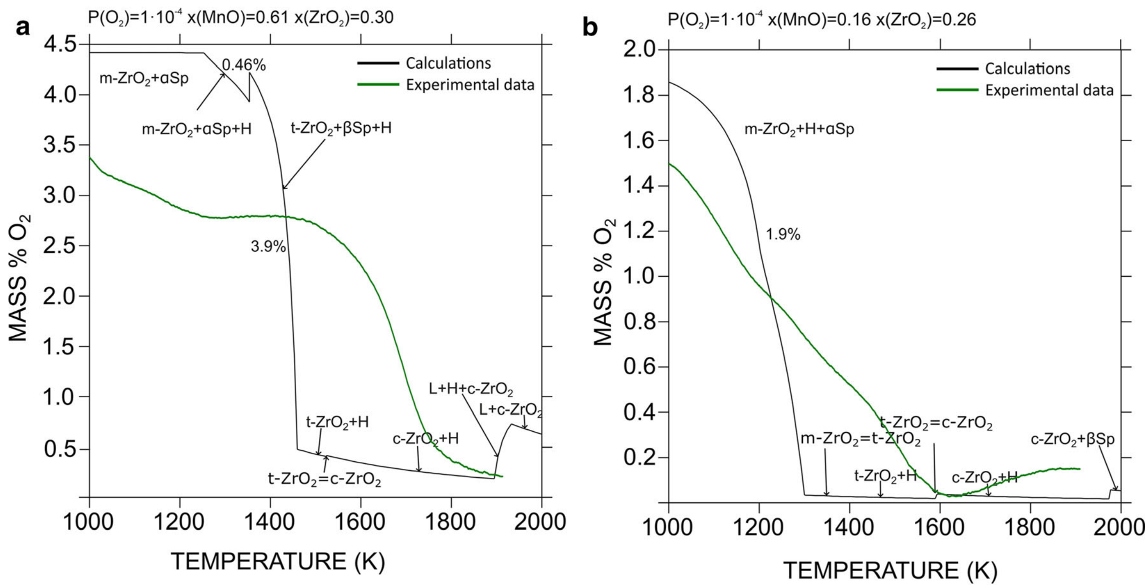


**Fig. 6** The calculated weight loss for compositions: (a) $ZrO_2$-8.67MgO-61.03$MnO_x$ and (b) $ZrO_2$-58.33MgO-16.08$MnO_x$ (in mol.%)

potential for the study of directionally solidified eutectic materials based on the $ZrO_2$-MgO-$MnO_x$ system.

**Acknowledgments** The authors thank the German Research Foundation (DFG) for funding Sub-project C2 within the Collaborative Research Center SFB 799 Trip-Matrix Composites. In addition, we thank G. Savinykh for technical contribution.

**Funding** Open Access funding provided by Projekt DEAL.



## References

1. H. Biermann, U. Martin, C.G. Aneziris, A. Kolbe, A. Müller, W. Schärfl, and M. Herrmann, Microstructure and Compression Strength of Novel TRIP-Steel/Mg-PSZ Composites, *Adv. Eng. Mater.*, 2009, **11**(12), p 1000-1006
2. M. Kirschner, S. Martin, S. Guk, U. Prahl, and R. Kawalla, Forming Complex Graded and Homogeneous Components by Joining Simple Presintered Parts of TRIP-Matrix Composite Through Powder Forging, *Metals*, 2020, **10**(4), p 543
3. S. Martin, Private communication, 2020
4. G. Bayer, Stabilization of Cubic $ZrO_2$ by MnO and Partial Substitution of Ti, Nb, or Ta for Zr, *J. Am. Ceram. So.*, 1970, **53**(5), p 294
5. H. Berek, A. Yanina, C. Weigelt, and C.G. Aneziris, Determination of the Phase Distribution in Sintered TRIP-Matrix/Mg-PSZ Composites Using EBSD, *Steel Res. Int.*, 2011, **82**(9), p 1094-1100
6. A. Orera, J.I. Peña, S. Serrano-Zabaleta, A. Larrea, and V.M. Orera, Fibrillar $Mn_3O_4$–YMnSz Well-Ordered Eutectics with Potential Functional Applications, *J. Eur. Ceram. Soc.*, 2015, **35**(3), p 909-918
7. W.J. Minford, R.C. Bradt, and V.S. Stubican, Crystallography and Microstructure of Directionally Solidified Oxide Eutectics, *J. Am. Ceram. Soc.*, 1979, **62**(3–4), p 154
8. D. Pavlyuchkov, D. Dilner, G. Savinykh, and O. Fabrichnaya, Phase Equilibria in the $ZrO_2$-MgO-$MnO_x$ System, *J. Am. Ceram. Soc.*, 2016, **99**(9), p 3136-3145
9. D. Pavlyuchkov, G. Savinykh, and O. Fabrichnaya, Experimental Investigation and Thermodynamic Modeling of the $ZrO_2$-MgO System, *Adv. Eng. Mater.*, 2013, **15**(7), p 618-626
10. D. Pavlyuchkov, G. Savinykh, and O. Fabrichnaya, Experimental Investigation and Thermodynamic Modeling of the $ZrO_2$–MnO System, *J. Eur. Ceram. Soc.*, 2015, **35**(13), p 3623-3632
11. D. Dilner, D. Pavlyuchkov, T. Zienert, L. Kjellqvist, and O. Fabrichnaya, Thermodynamics of the Mg-Mn-O System-MODELING and Heat Capacity Measurements, *J. Am. Ceram. Soc.*, 2017, **100**(4), p 1661-1672
12. L. Kjellqvist and M. Selleby, Thermodynamic Assessment of the Fe-Mn-O System, *J. Phase Equilib. Diffus.*, 2010, **31**(2), p 113-134
13. A.N. Grundy, B. Hallstedt, and L.J. Gauckler, Assessment of the Mn-O System, *JPE*, 2003, **24**(1), p 21-39
14. L. Lutterotti, Total Pattern Fitting for the Combined Size–Strain–Stress–Texture Determination in Thin Film Diffraction, *Nucl. Instrum. Methods Phys. Res., Sect. B*, 2010, **268**(3–4), p 334-340
15. M. Hillert, B. Jansson, B. Sundman, and J. Ågren, A Two-Sublattice Model for Molten Solutions with Different Tendency for Ionization, *Metall Mat Trans A*, 1985, **16**(2), p 261-266

16. B. Sundman, Modification of the Two-Sublattice Model for Liquids, *Calphad*, 1991, **15**(2), p 109-119
17. M. Hillert, The Compound Energy Formalism, *J. Alloy. Compd.*, 2001, **320**(2), p 161-176
18. O. Fabrichnaya and D. Pavlyuchkov, Assessment of Experimental Data and Thermodynamic Modeling in the Zr-Fe-O System, *Metall and Mat Trans A*, 2016, **47**(1), p 152-159
19. B. Hallstedt, The Magnesium—Oxygen system, *Calphad*, 1993, **17**(3), p 281-286
20. A. Kuprava, I. Saenko, and O. Fabrichnaya, Heat capacity Measurement of C14–$ZrMn_2$ and Thermodynamic Re-assessment of the Mn–Zr System, *Calphad*, 2020, **68**, p 101745
21. M. Hämäläinen and K. Zeng, Thermodynamic Evaluation of the Mg-Zr System, *Calphad*, 1998, **22**(3), p 375-380
22. J. Tibballs, I. Ansara, A.T. Dinsdale, M.H. Rand, Ed., *COST 507, Thermochemical Database for Light Metal Alloys, vol. 2, EUR 18499, 1998, 215–217*
23. Y. Yin and B.B. Argent, Phase Diagrams and Thermodynamics of the Systems $ZrO_2$-CaO and $ZrO_2$-MgO, *JPE*, 1993, **14**(4), p 439-450
24. P. Duran, J.M. Rodriguez, and P. Recio, The $ZrO_2$-Rich Region of the $ZrO_2$-MgO System, *J. Mater. Sci.*, 1991, **26**(2), p 467-472
25. F. Ebert and E. Cohn, Beitrge zur Keramik hochfeuerfester Stoffe. VI. Das system $ZrO_2MgO$, *Z. Anorg. Allg. Chem.*, 1933, **213**(4), p 321-332
26. C.F. Grain, Phase Relations in the $ZrO_2$-MgO System, *J. Am. Ceram. Soc.*, 1967, **50**(6), p 288-290
27. S.M.O. Sim and V.S. Stubican, Phase Relations and Ordering in the System $ZrO_2$-MgO, *J. Am. Ceram. Soc.*, 1987, **70**(7), p 521-526
28. T. Kawashima, Phase Equilibria in $ZrO_2$–$Y_2O_3$–$MnO_t$ Ternary System at 1673 K, *Mater. Trans. JIM*, 1999, **40**(9), p 967-971
29. R.L. Shultz and A. Muan, Phase Equilibria in the System MnO-"FeO"-$ZrO_2$-$SiO_2$, *J. Am. Ceram. Soc.*, 1971, **54**(10), p 504-510
30. SGTE Substance Database. https://www.sgte.net/ (accessed 24 June 2020)
31. C. Wang, M. Zinkevich, and F. Aldinger, The Zirconia-Hafnia System: DTA Measurements and Thermodynamic Calculations, *J. Am. Ceram. Soc.*, 2006, **89**(12), p 3751-3758
32. H. Biermann, TRIP-Matrix-Composites, *Adv. Eng. Mater.*, 2019, **21**(5), p 1900126